### Title

Impact of temperature on the pullout of reinforcing geotextiles from unsaturated silt




### Journal

Geosynthetics International, 27(1)

### ISSN

1072-6349



### Authors

Ambriz, B

Mun, W

McCartney, JS



### Publication Date

2020-02-01

### DOI

10.1680/jgein.19.00040

Peer reviewed

# Impact of temperature on the pullout of reinforcing geotextiles from unsaturated silt

**Bernardo Ambriz[1], Woongju Mun[2], John S. McCartney[3]**

*[1] Staff Engineer, Earth Mechanics, Inc., 3541 Investment Blvd. #4, Hayward, CA 94545, USA; Telephone: +1/510 562 8833; E-mail: b.ambriz@earthmech.com.*

*[2] Senior Staff Engineer and Laboratory Research Scientist, Hushmand Associates, Inc., 250 Goddard, Irvine, CA. Telephone: 1/303-522-2701. E-mail: musim21@gmail.com.*

*[3] Professor and Department Chair, Department of Structural Engineering, University of California, San Diego, La Jolla, CA, 92093-0085, USA; Telephone: +1/858-534-9630; E-mail: mccartney@ucsd.edu; ORCID Number: 0000-0003-2109-0378 (Corresponding Author).*

**ABSTRACT**: This study investigates the thermal soil-geosynthetic interaction mechanisms of reinforcing geotextiles confined in compacted silt that may be encountered when using mechanically-stabilized earth (MSE) walls as geothermal heat sinks. A thermo-mechanical geosynthetic pullout device was used that incorporates standard components for geosynthetic pullout or creep testing but also heating elements at the top and bottom of the soil box to apply boundary temperatures and dielectric sensors embedded in the soil layer to monitor distributions in temperature and volumetric water content. Two test series were performed: the first involves monotonic pullout of woven polypropylene geotextiles after reaching steady-state conditions under different boundary temperatures without a seating load, and the second involves monotonic pullout of woven polyethylene-terephthalate geotextiles after reaching steady-state conditions under different boundary temperatures with a seating pullout load. The results indicate that the pullout resistance of both geotextiles decreased with increasing temperature. Although heating led to drying of the unsaturated silt layers as expected, measurements from the second test series indicate accumulation of water at the silt-geotextile interface. An effective stress analysis considering thermal softening of soils indicates that the increase in effective saturation at the silt-geotextile interface was the cause of the decrease in pullout resistance with heating.

**KEYWORDS**: Geosynthetics, Thermo-mechanical pullout device, unsaturated soil, nonisothermal behavior, geotextiles, thermal softening.

## 1. INTRODUCTION

Mechanically-Stabilized Earth (MSE) walls are cost-effective soil retaining structures that can tolerate relatively large settlements or facing displacements without reaching failure (Berg et al. 2009). The underlying concept of MSE walls is the placement of tensile reinforcing elements (i.e., geogrids, geotextiles, metallic strips, etc.) during compaction of backfill soil to form a self-

supporting system. The internal stability and deformation response of MSE walls depend on the tensile strength and creep characteristics of the reinforcements, the shear strength of the interface between the reinforcements and the backfill soil, and soil-geosynthetic interaction. Infiltration and evaporation into the backfill due to environmental interaction along with changes in the groundwater table may play an important role in the deformation response of MSE walls, as additional water will increase the backfill self-weight and reduce the effective stress in the backfill. Decreases in effective stress of unsaturated soils may lead to corresponding decreases in shear strength and shear modulus (e.g., Lu et al. 2010; Khosravi and McCartney 2012).

To minimize issues arising from changes in the backfill effective stress state, MSE wall design methodologies specify the use of free-draining backfill soils having low fines content (less than 15%) within the reinforced zone (e.g., Berg et al. 2009). However, in some cases, free-draining soils are not readily available or may be too expensive for a project. Although not permitted in most design specifications, it may be possible to use non-ideal, poorly-draining backfill soils with higher fines content that may be available on site with appropriate engineering considerations. A few studies have found that under optimal conditions these poorly draining backfill soils can have acceptable performance, especially when they remain unsaturated (Zornberg and Mitchell 1994; Zornberg et al. 1995). Engineering approaches that have been used to maintain unsaturated conditions in backfill soil in MSE walls include proper grading of the wall crest along with water diversion elements, inclusion of toe or chimney drains in the backfill, or the use of capillary barriers within the backfill soil (Iryo and Rowe 2005; Zorberg et al. 2010; Portelinha and Zornberg 2017). A novel approach to reduce the negative effects of using poorly-draining backfill soils in MSE walls is to incorporate geothermal heat exchangers into MSE walls to induce drying of backfill soils by thermally-induced water flow. Specifically, different configurations of earth

structures with geothermal heat exchangers have been proposed, including thermally-active MSE walls (Stewart and McCartney 2013; Stewart et al. 2014a) and thermally-active embankments (Coccia and McCartney 2013). In addition to helping maintain the backfill soil in unsaturated conditions, these systems can be used to dissipate excess heat from adjacent buildings or industry, making cooling systems become more environmentally friendly. Integrating MSE walls into the energy infrastructure may make their construction more economical by offsetting costs associated with cooling requirements. As MSE walls already incorporate several subsurface technologies including geosynthetics and drainage components, inclusion of plumbing for geothermal heat exchangers is not expected to create a significant increase in their construction cost or complexity.

One challenge encountered when incorporating geothermal heat exchangers into MSE walls is that heat transfer may lead to a change in the behavior of the soil and geosynthetic reinforcements, which must be understood before this technology is implemented in practice. As mentioned, thermally-induced flow of water is expected to occur in unsaturated soils from zones of high temperature (i.e., at the geothermal heat exchangers) to zones of lower temperature due to a combination of water phase change and enhanced vapor diffusion (i.e., Philip and De Vries 1957; Başer et al. 2018). This will lead to a lower degree of saturation, increased suction, and increased effective stress in the backfill soil at the locations of the heat exchangers (Coccia and McCartney 2013). In addition to the improvement in shear strength and shear modulus associated with increasing effective stress, an increase in suction also leads to an increase in yield stress, which is referred to as suction hardening (Khosravi and McCartney 2012). If geotextiles are used as the reinforcing geosynthetic in the MSE wall they may also act as lateral vapor drains, helping to expel water from the backfill (Stewart et al. 2014b). The ability of a geotextile to act as a vapor drain will depend on the polymer as well as if the geotextile is woven or nonwoven (Stormont and Ramos

2004; Stormont et al. 2010; Lin et al. 2018). Despite the positive effects of heating, it is well known that heating of geosynthetics in unconfined conditions (Zornberg et al. 2004; Bueno et al. 2005) or confined conditions (Karademir 2011) may lead to accelerated creep deformations. This may lead to additional lateral displacements in thermally-active MSE walls, which can be referred to as thermal softening (Stewart et al. 2014a). Although it is well accepted that temperature does not affect the compression indices and critical state friction angle of soils (Campanella and Mitchell 1968; Laloui et al. 2014), elevated temperatures also may lead to volumetric contraction in unsaturated soils (Coccia and McCartney 2016a, 2016b) and a thermal softening effect leading to a reduction in the peak shear strength and stiffness (Uchaipichat and Khalili 2009). The interaction between the effects of heat transfer and water flow on the effective stress state in unsaturated soils and the thermal softening of the geosynthetic reinforcements and soil must be carefully considered. Specifically, it is important to consider the behavior of geosynthetics confined in unsaturated backfill soil under nonisothermal conditions when determining whether the positive influence of a decreased degree of saturation in the backfill soil (and greater effective stress) offsets the negative influence of thermal softening.

The objective of this study is to characterize the interaction between woven reinforcing geotextiles and unsaturated, poorly-draining backfill soil during application of different temperatures to the boundaries of a pullout device. Soil-geosynthetic interaction will be evaluated in terms of both the load-displacement pullout curve and the ultimate pullout resistance. Further, measurements of the spatial and temporal changes in temperature, volumetric water content (and indirectly the matric suction), and volume change in the soil under different temperature boundary conditions will be used to understand the transient heat transfer and water flow processes in the

unsaturated soil, and this information will be integrated into an effective stress analysis to interpret the nonisothermal pullout results.

The tests in this study were performed using a thermo-mechanical pullout device originally developed by Carpenter et al. (2015) that was updated to perform creep tests under a constant mechanical load and pullout tests at a constant displacement rate. The pullout device incorporates standard components including a rigid pullout box with an integrated vertical loading system, a roller grip to apply pullout forces uniformly to the geotextiles, a pulley system for load-controlled creep testing, a servo-motor for displacement controlled monotonic pullout testing, and instrumentation for monitoring vertical settlement, pullout force, and pullout displacement measurements. The pullout box also incorporates heating elements at the top and bottom of the box, along with an array of dielectric sensors embedded in the soil for measurement of temperature and volumetric water content. As the reinforcing geosynthetic is placed at mid-height of the pullout box, the heaters at the top and bottom of the box simulate the case of a thermally-active MSE wall where horizontal heat exchangers are placed in the backfill at intermediate lifts between the lifts containing reinforcing geosynthetics. Accordingly, heat transfer and water movement will be toward the reinforcing geosynthetic, so this testing approach also permits evaluation of the role of woven geotextiles as lateral drains for water vapor.

## 2. BACKGROUND

### 2.1 Effective Stress in Unsaturated Soils

Like saturated soils, unsaturated soils change in volume due in response to changes in effective stress. Because unsaturated soils are a three-phase system, mechanical deformation and hydraulic changes take place simultaneously under external loads, with the degree of saturation playing an

important role in the soil behavior (Sun et al. 2010). The effective stress definition of Bishop (1959) was used in this study, where the mean effective stress p′ is expressed as follows:

$$p' = p_{net} + \chi\psi \quad (1)$$

where $p_{net}$ is the mean net stress equal to the difference between the mean total stress p and the pore air pressure $u_a$, $\psi$ is the matric suction equal to the difference between the pore air pressure $u_a$ and pore water pressure $u_w$, and $\chi$ is the effective stress parameter. The effective stress parameter is assumed to equal the effective saturation ($\chi = S_e$) following the approach of Bolzon et al. (1996), as Lu et al. (2010) found that this approach permits integration of the soil-water retention curve (SWRC) into the effective stress definition. The SWRC of Grant and Salehzadeh (1996) was used in this study as it permits consideration of the effects of temperature on the SWRC, and is given as follows:

$$S_e = \frac{S_r - S_{r,res}}{1 - S_{r,res}} = \left\{ \frac{1}{\left[\alpha_{GS}\psi\{(\beta_0 + T_r)/(\beta_0 + T_f)\}\right]^{\lambda_{GS}} + 1} \right\}^{(\lambda_{GS}-1)/\lambda_{GS}} \quad (2)$$

where $S_r$ is the degree of saturation, $S_{r,res}$ is the residual saturation, $T_r$ is the initial reference temperature in K, $T_f$ is the final temperature in K, $\beta_0$ is an empirical constant, and $\alpha_{GS}$ and $\lambda_{GS}$ are fitting parameters. A value of $\beta_0$ equal to -400K was used in this analysis, as Grant and Salehzadeh (1996) found that this is representative of silty soils. Substitution of Equation (2) into Equation (1) by assuming $\chi$=$S_e$ permits definition of an effective stress value for unsaturated soils that varies with the effective saturation and temperature. Further, the matric suction in soil can be estimated from measured values of temperature and degree of saturation using Equation (2).

## 2.2 Soil-Geosynthetic Interaction

The tensile stress-strain behavior of a geosynthetic is often represented in terms of a force per unit width versus displacement curve as they are planar in structure. The tensile stiffness of

148 geosynthetics is typically defined as the tangent slope of the force-displacement curve in the elastic
149 region, whereas their ultimate tensile strength is defined as the maximum load before rupture.
150 Although the tensile strength of a geosynthetic is the primary variable used in the design of MSE
151 walls, the effects of the confining stress induced by the soil may affect the geosynthetic. McGown
152 et al. (1982) measured the tensile strength of geotextiles under confined and unconfined conditions
153 and found that the stiffness of the geotextile increased with an increase in confining pressure.
154 Bueno et al. (2005) noted that the confining pressure prevents necking (or reduction in transverse
155 strains) of the geosynthetic leading to higher stiffness. Temperature may also affect the tensile
156 behavior of geosynthetics. Changes in tensile stiffness of a geosynthetic with temperature depend
157 on the polymer, as different polymers have different glass transition temperatures $T_g$. At the glass
158 transition temperature, a transition from a brittle to a viscous response is expected, resulting in a
159 change in stiffness. Although no change in stiffness is expected if the glass transition temperature
160 is not exceeded, the elevated temperature may still lead to tensile creep deformations (Zornberg et
161 al. 2004; Bueno et al. 2005; Karademir 2011).

162 Soil-geosynthetic interaction mechanisms are typically assessed using geosynthetic pullout
163 tests. These tests involve application of tensile stresses to a reinforcing geosynthetic confined in a
164 layer of compacted soil to characterize the pullout resistance. The minimum dimensions of a
165 pullout box for geosynthetic pullout are defined in ASTM D6706, which were defined to minimize
166 boundary effects that can affect the pullout response. Side wall boundary effects occur when
167 frictional resistance is mobilized along the side walls of the pullout box. Farrag et al. (1993)
168 evaluated the impact of the side wall effects as a function of the distance from the edge of the
169 geosynthetic to the side walls. They found that greater side wall distances reduced the frictional
170 resistance, and that the confining stress played a major role in this boundary effect. The top and

bottom plates of a pullout box may have similar effects as the side walls due to the mobilization of the soil along with the interface caused by friction. Brand and Duffy (1987) studied the effects of the soil cover height on the pullout response of geogrids and found that for soil cover heights greater than 65 mm, the soil cover effect was minimized. Passive pressure between the soil and the front wall of the pullout box may also affect the pullout response. This effect can be mitigated by installing bearing sleeves attached to the top and bottom opening to reduce front wall boundary effect. Chang et al. (2000) performed an investigation on the effects of the sleeve lengths and found that after including bearing sleeves with a length of 15 mm there were minimal effects to the measured pullout resistance. Back wall boundary effects are typically not expected to have a major effect on pullout, but some space should be provided if the backfill has an apparent tensile strength like that associated with unsaturated conditions.

Several studies have investigated the pullout of reinforcing geosynthetics from unsaturated, marginal, fine-grained backfill soils (Lee and Bobet 2005; Zornberg et al. 2005; Yoo et al. 2007; Clancy and Naughton 2011; Hatami et al. 2013; Esmaili et al. 2014; Hatami and Esmaili 2015). These studies indicate that less interlocking between the soil and geosynthetics occurs in fine-grained backfills compared to granular backfills, and that lower pullout resistances are observed for higher gravimetric water contents (and lower suctions). However, several studies found that providing drainage to fine-grained backfill soils may compensate for any reductions in interaction with higher water content (Zornberg and Kang 2005; Yoo et al. 2007; Clancy and Naughton 2011). For this reason woven or nonwoven geotextiles are typically used as the reinforcing geosynthetic in fine-grained backfill soils as they provide better drainage than geogrids, although specialty geosynthetics like geogrids with embedded drains or geocomposites may also be used. Direct shear testing of the interface between unsaturated soils and geotextiles by Khoury et al. (2011) and

Jotisankasa and Rurghaisri (2018) indicate that the apparent cohesion induced by unsaturated conditions will lead to an increase in interface shear strength. They observed that the increase in apparent cohesion may vary nonlinearly with suction. Hatami and Esmaili (2015) found that the pullout resistance of woven geotextiles in different unsaturated soils decreases linearly with increasing gravimetric water content for values ±2% of optimal gravimetric water content, while Esmaili et al. (2014) showed linear increases in shear strength interpreted from pullout tests with suction. These studies obtained different initial combinations of suction and water content through compaction, and noted that soil structure associated with compaction may play a role in the results.

## 3. EXPERIMENTAL SETUP

Schematics of the thermo-hydro-mechanical pullout device used in this study are shown in Figures 1(a) and 1(b), while a photograph of the device is shown in Figure 1(c). The main difference between the device used in this study and the original device developed by Carpenter et al. (2015) are the approaches to apply pullout loads to geosynthetics in both load-control conditions (i.e., to evaluate creep under constant load) and in displacement-control conditions (i.e., to evaluate monotonic pullout to failure). The pullout load is applied to the geosynthetic using a combination of a dead-weight system, which facilitates evaluating creep under constant load, and a linear actuator, which facilitates monotonic geosynthetic pullout. A roller grip on a sliding frame is used to grip the geosynthetic to apply uniform horizontal pullout loads. A Bellofram pneumatic piston is used to apply vertical loads to a rigid plate on the top of the soil specimen. Although application of vertical stresses using a rigid plate may lead to stress concentration issues, the top plate of the pullout device contains heat exchange tubing as will be mentioned later.

Plan- and elevation-view schematics showing the internal dimensions of the soil container are shown in Figure 2, along with the locations of instrumentation embedded in the soil mass. Pictures

of the inside of the container and the placement of instrumentation are shown in Figure 3. Dielectric sensors (model 5TM from Decagon Devices) were embedded at different depths and were used to monitor changes in both temperature and volumetric water content in the soil layers during heating. Since the apparatus is not designed to control the suction within the soil layers during testing, the dielectric sensors are used to infer changes in volumetric water content during the heating process, and the suction can be inferred using the SWRC using Equation (2). A long-stroke (150 mm) linearly variable differential transformer (LDVT) was used to measure the displacements of the grip. Although internal displacements were measured using tell-tales by Carpenter et al. (2015), the displacements were relatively small during heating indicating that negligible thermal creep occurred in the confined geotextile. Accordingly, the were not used in this study and the grip displacements were used to interpret the pullout response. S-type load cells were used to monitor the vertical force applied by the Bellofram piston and the horizontal pullout force, and two vertical LDVTs were used to measure the settlement and possible tilting of the top cap. The bottom of the soil container contains a 12 mm-thick Delrin plate with an embedded copper heating coil as shown in Figure 3(a). The top plate of the device also includes a 12 mm-thick Delrin plate with an embedded copper heating coil beneath an aluminum plate as shown in Figure 3(d) and was designed to allow vertical stresses to be applied via the Bellofram piston while still permitting temperatures to be applied to the top of the soil layer. Delrin was used to constrain the heating coils as it has a low thermal conductivity compared to that of the aluminum plates.

The temperature of the soil can be controlled by circulating water through the copper heating coils at both the top and the bottom of the soil layer. The heating coils do not extend across the entire top or bottom width of the loading plates but were placed in a spiral form across the center of the plate. This means that the soil within 75 mm of the front and back edges of the container are

not directly heated. However, the interaction zone of the geosynthetic was expected to only be in the center portion of the soil box due to both the presence of the passive bearing sleeve at the face of the container and the fact that the geosynthetic did not extend all the way to the back of the container, as shown in Figure 2(b). An advantage of this approach was that the geosynthetic loading system (i.e., roller grips and unconfined geosynthetic) were unheated, minimizing the effects of thermally-induced creep of the unconfined geosynthetic. A circulating heat pump (model F25-Me from Julabo, Inc) was used to control the temperature of the water circulating through the closed-loop copper coils in the loading plates to reach the desired boundary temperatures. The actual temperatures of the fluid entering and exiting the copper coils on the top and bottom of the container are measured using pipe-plug thermocouples (model TC-T-NPT-G-72 from Omega).

## 4. MATERIALS

### 4.1 Soil and Specimen Preparation Details

Bonny silt was used in the tests performed in this study, which has a Unified Soil Classification Scheme (USCS) classification of ML (inorganic silt). The geotechnical properties of the silt are summarized in Table 1. Bonny silt was used in this study as it is an example of a poorly draining backfill that does not meet specifications for use in MSE walls (Berg et al. 2009), and because it has been widely characterized in other studies (Khosravi and McCartney 2012; Vega and McCartney 2015; Coccia and McCartney 2016a, 2016b).

The silt was compacted into the pullout box using an impact hammer to a target dry density of 14.2 kN/m$^3$ at a target gravimetric water content of 13.9%. For these compaction conditions, the thermal conductivity of the silt was 1.2 W/(mK), which was measured following ASTM D5334 using a KD2Pro thermal needle from Decagon Devices. The soil-water retention curve (SWRC) for Bonny silt at different temperatures was represented using the Grant and Salehzadeh (1996)

263 model, as shown in Figure 4. It was observed that an increase in temperature leads to a slight
264 downward shift in the SWRC implying that the soil retains less water under higher temperatures
265 for the same suction. Figure 4 also includes the suction stress characteristic curves (SSCCs)
266 defined using the approach of Lu et al. (2012) [i.e., the suction stress is the product of $S_e$ and $\psi$ in
267 Equation (1)] predicted from these SWRCs using the model of Lu et al. (2010) are also shown in
268 Figure 4. The lower suction stress with increasing temperature indicates that for a given matric
269 suction, the effective stress will decrease as the soil is heated.

270 ## 4.2 Geosynthetics

271 Two geosynthetics were used in the testing program and their properties are given as the
272 following. The first geosynthetic used in this study is a woven polypropylene (PP) geotextile
273 manufactured by TenCate-Mirafi Inc. (product name Mirafi 600X, referred to as Geotextile A),
274 and the second geosynthetic used in this study is a woven polyethylene terephthalate (PET)
275 geotextile manufactured by TenCate-Mirafi Inc. (product name Mirafi PET70/70, referred to as
276 Geotextile B). Relevant properties of both geotextiles are summarized in Table 2. The goal of this
277 study was not to compare the response of the two geotextiles as the details of the testing series for
278 each geotextile are different and the geotextiles have very different values of ultimate tensile
279 strength, glass transition temperatures, and pullout resistances from compacted silt at room
280 temperature. However, the lessons learned from the impacts of heating on the pullout response of
281 both geotextiles help understand the complex thermo-hydro-mechanical soil-geosynthetic
282 interaction. It was not expected that the geotextiles would provide a significant impedance to water
283 vapor diffusion as they both have high permittivity.
284

## 5. EXPERIMENTAL PROCEDURES

The soil was prepared in 50 mm-thick lifts using dynamic compaction with an impact hammer. The soil was compacted directly on top of the heating coils on the bottom of the container. The dielectric sensors were placed at the interfaces between lifts, ensuring that the sensors were horizontal. The sensors were placed in such a manner that the cable would not provide any tensile resistance to the pullout, as shown in Figure 3(b). The sensor wires are routed to exit from the back of the container with a bend in the cable to again ensure that they do not provide tensile resistance during pullout testing. The sensors exit from a hole in the side of the container to avoid damage when applying the vertical stress. The interfaces between the layers were scarified to minimize the formation of weak zones within the layers. After compaction of the soil sample, the top surface was carefully leveled to ensure the top plate would apply a uniform stress to the soil along with applying a uniform boundary temperature. Negligible tilting was observed during compression and pullout, which indicated that relatively uniform stresses were applied through the entirety of the study. A vertical stress of 19.5 kPa was applied in all tests, and typical settlement results shown in Figure 5 indicate that the end of primary consolidation was reached in less than 24 hours.

Two testing series were performed in this study, as summarized in Table 3. The first testing series involved the PP geotextile, while the second testing series involved the PET geotextile. The two testing series were performed sequentially, and the details of the second testing series were refined to investigate issues observed in the first testing series. In the first testing series, no seating pullout load was applied to the geotextile, and monotonic pullout was performed after reaching steady-state conditions in terms of heat transfer and water flow in the unsaturated soil layer. In the second series, a seating pullout load was applied using a dead weight pulley system to understand if thermally-induced creep may affect the pullout response, after which monotonic pullout was

performed after reaching steady-state conditions. In both testing series, after consolidation of the soil, the heat pump was turned on and set to the desired boundary condition temperature. The specimens were then monitored for 7 days to allow the soil to reach steady-state conditions. When performing the monotonic pullout portion of the tests, the pullout loads were applied in displacement-control conditions at a constant rate of 0.0215 mm/min using the linear actuator until reaching the pullout resistance.

## 6. RESULTS

The tests on the PP geotextile in Series 1 involved application of boundary temperatures ranging from 20 to 50 °C with an initial average soil temperature of 23.4 °C. The changes in temperature of the soil 13 mm below the soil-geosynthetic interface during the heating/cooling period are shown in Figure 6(a). The temperature of the soil was observed to increase (or decrease) rapidly, reaching steady state within 2 days. The changes in volumetric water contents ($\Delta\theta_w$) inferred from the dielectric sensors and corrected for temperature effects using the model of Iezzoni and McCartney (2015) are shown in Figure 6(b). As expected, heating of the soil causes drying of the silt, leading to a larger change in volumetric water content with higher temperatures. The volumetric water contents required longer durations to reach steady-state than the temperatures. Pullout had a negligible effect on the change in volumetric water content. The change in effective stress of the soil 13 mm below the soil-geosynthetic interface calculated using Equations (1) and (2) using the dielectric sensor measurements are shown in Figure 6(c). The initial effective stress shown in this figure includes the applied stress, the self-weight of the soil overlying the geotextile (2.7 kPa), and the initial suction stress corresponding to the unsaturated conditions in the soil layer at room temperature (27.4 kPa target compaction conditions noted above). At this location, the effective stress increases during heating up to nearly 10% of the initial effective stress

331 due to the coupled heat transfer and water flow in the soil layer, with a greater increase in effective
332 stress with increasing temperature. The test with a decrease in temperature to 20 °C showed a slight
333 decrease in effective stress. This increase in effective stress during heating is expected to lead to
334 both an increase in peak shear strength and an increase in stiffness of the soil. The change in void
335 ratio of the soil layer is shown in Figure 6(d). Consistent with the observations of Coccia and
336 McCartney (2016b), heating of the unsaturated silt led to contraction. Greater contractions are
337 observed for greater boundary temperatures. Pullout led to negligible changes in volume based on
338 the observations at the box boundary.

339 The temperature profiles at the end of the heating/cooling phase from the Series 1 tests are
340 shown in Figure 7(a). The temperature values were obtained from the dielectric sensors embedded
341 in the soil and from the averages of the fluid temperatures entering and exiting the top and bottom
342 copper heat exchanger coils. In the Series 1 tests, the temperatures on the top and bottom of the
343 box were approximately equal, and the temperatures within the soil layer were generally the
344 topmost and bottommost temperature measurements are approximately equal to the targeted
345 boundary temperatures confirming that the boundary temperatures were the same in this series of
346 tests. The corresponding change in volumetric water content (i.e., from the start of heating to
347 immediately before geotextile pullout) measured from the dielectric sensors and the actual
348 volumetric water contents from physical sampling of the soil at the end of the testing are shown in
349 Figures 7(b) and 7(c), respectively. In general, more drying was observed for higher temperatures,
350 and more drying occurred closer to the heat exchanger coils at the top and bottom of the pullout
351 box. Note that the initial volumetric water contents before heating were approximately uniform
352 and equal to 0.20. The profiles in Figure 7(b) and 7(c) have slightly different shapes as the

353 sampling of the soil did not occur until after the specimen was disassembled, while the changes in
354 volumetric water content from the dielectric sensors were immediately prior to pullout.

355 The pullout force-displacement curves for the four Series 1 tests are shown in Figure 8. Not
356 only is a decrease in pullout resistance with temperature observed in this figure, but the slope of
357 the curves slightly decreases with increasing temperature. These observations are contrary to the
358 expectation that the drying of the soil observed in Figures 6 and 7 with increased temperature
359 would lead to an increase in peak shear strength of the soil and thus the geotextile pullout
360 resistance. Although the curves in Figure 8 seem to indicate that thermal softening may have been
361 the cause of the decrease in pullout resistance, this testing series was performed without a seating
362 pullout load and there was no evidence that the increase in temperature affected the stiffness of the
363 PP geotextile (even though all the temperatures applied were greater than the PP geotextiles glass
364 transition temperature). Further, the water content of the soil directly at the soil-geosynthetic
365 interface was not measured in this testing series, so even though the dielectric sensor measurements
366 in Figure 6 were from 13 mm below the geotextile, the soil at the interface may have had a different
367 response. Accordingly, the lack of a conclusive explanation for the trends observed for the curves
368 from Series 1 in Figure 8 provided the motivation for performing the second testing series with a
369 seating pullout load and more discrete sampling of the water content profile near the soil-
370 geosynthetic interface.

371 The tests on the PET geotextiles in Series 2 involved application of a seating pullout load of
372 1.43 kN/m after consolidation but before application of the different temperatures to the
373 boundaries of the pullout box. The pullout load was maintained for 24 hours to permit any
374 mechanical creep to occur before the start of heating. However, negligible mechanical pullout

creep displacements were observed, possibly because the applied seating load is only 10% of the pullout resistance measured in a monotonic test at room temperature on this geotextile.

In Series 2, only three elevated target temperatures were analyzed (30, 40, and 50 °C) in addition to a room temperature test at a temperature of 23.2 °C. A reference test at room temperature without a seating load was also performed (Test 2.1). Similar to the Series 1 tests, the soil temperature 13 mm below the soil-geotextile interface in the Series 2 tests reached steady state within one day of starting the heating pump, as shown in Figure 9(a). The change in volumetric water content versus time 13 mm below the soil-geotextile interface is shown in Figure 9(b). Although drying was observed at this location in all three heated Series 2 tests, the tests at 40 and 50 °C showed an initial increase (wetting) at this location followed by a decrease. Further, the magnitude of the overall decreases in volumetric water content at this location was also smaller in the Series 2 tests compared to the decreases observed in the Series 1 tests. This may have been due to slight differences in the top and bottom boundary temperatures, as will be discussed later. Although a slight increase in effective stress is observed 13 mm below the geotextile in the test at a target temperature of 30 °C in Figure 9(c), a decrease in effective stress followed by an increase was observed in the tests at target temperatures of 40 and 50 °C. The trend in effective stress with time in the two tests at higher target temperatures is due to both the increasing and decreasing trend in the change volumetric water content observed these tests and to the effects of temperature on the matric suction estimated from the SWRC in Equation (2). The latter effect caused the change in effective stress at the time of pullout for the test at a target temperature of 50 °C to be slightly lower than in the test at a target temperature of 40 °C. The void ratios of the soil layers during heating obtained from the settlements of the top plate are shown in Figure 9(d). Similar to the observations from the Series 1 tests, contraction was observed in all the tests. However, no clear

398 relationship between the change in void ratio and boundary temperature was observed in this
399 testing series.

400 The pullout creep displacements during heating of the PET geotextiles in the Series 2 tests are
401 shown in Figure 10. The thermal creep displacements showed some noise due to the small
402 magnitude, but generally showed an asymptotic trend to a stable value with. The thermal creep
403 displacements in the Series 2 tests followed the proposed hypothesis from Stewart and McCartney
404 (2013), where higher temperatures resulted in greater pullout creep displacements. However, the
405 magnitude of pullout creep displacements from these tests were small compared to the pullout
406 displacements required to reach the pullout resistance (i.e., approximately 5% of the displacement
407 at the pullout resistance). The small creep displacements observed in Figure 10 may be because
408 the applied temperatures are below the glass transition temperature for the PET geotextile.

409 The temperature profiles at the end of the heating phase for the Series 2 tests are shown in
410 Figure 11(a). A slight difference in temperature at the top in the bottom of the soil layers is
411 observed in these tests, with a slightly higher temperature at the bottom of the box. This was caused
412 by improper balancing of the flow through the top and bottom heat exchanger coils in these tests.
413 The bottom boundary temperature was approximately 2-4 °C greater than the top boundary
414 temperature in these tests, which may have led to more upward water vapor flow in the soil layer.
415 The changes in volumetric water content inferred from the dielectric sensors and the volumetric
416 water contents measured from soil samples are shown in Figures 11(b) and 11(c), respectively.
417 Different from the sampling in the Series 1 tests, additional locations were sampled in the Series 2
418 tests to better discretize the volumetric water content at the geosynthetic location. The profiles of
419 volumetric water content from sampling in Figure 11(c) indicate that drying occurred in the lower
420 part of the soil layer but wetting occurred in the upper part of the soil layer. Further, the profiles

of the volumetric water content from sampling shown in Figure 11(c) indicate a sharp break between the upper and lower parts of the soil-geosynthetic interface. This may indicate that water was condensing and accumulated in the soil above the geotextile during heating. This may indicate that the PET geotextile was not acting as a lateral drain for water vapor. Measurements of the volumetric water content directly at the soil-geosynthetic interface were not made in Series 1 tests, so it is possible that the trends in the Figure 11(c) may also apply to the Series 1 tests.

The pullout force versus displacement curves for the Series 2 tests are shown in Figure 12. Curves for tests at room temperature with and without a seating pullout load of 1.43 kN/m are also included in this figure for reference, and the application of a seating pullout load did not lead to a major change in the pullout resistance at room temperature. Like the Series 1 tests, a decrease in the pullout resistance was observed with increasing temperature. To evaluate whether this trend is associated with thermal softening or the decrease in effective stress at the location of the geotextile, an effective stress analysis must be used.

## 7. ANALYSIS

Although the Series 1 tests did not provide sufficient information to fully understand the mechanisms of the changes in pullout resistance with temperature, it is worthwhile to compare the pullout resistance values from the Series 1 and Series 2 tests to understand possible similarities in the two testing series. Evaluation of the trends in pullout resistance with the change in temperature at the location of soil-geotextile interface in Figure 13 for both testing series indicates that the PET geotextile had a greater pullout resistance than the PP geotextile in all cases evaluated. Further, a decrease in pullout resistance was not observed until the change in temperature at the interface reached a certain value. However, the interesting observation from the results in Figure 13 is that at higher changes in temperature, the rates of decrease in the pullout resistance were similar. This

444 indicates that the dependence of the pullout resistance on the change in temperature is likely
445 affected more by temperature effects on the soil rather than temperature effects on the geotextile.
446 Specifically, even though the PP geotextile has a much smaller glass transition temperature than
447 the PET geotextile a similar change in pullout resistance with temperature was observed for both
448 geotextiles.

449 The pullout resistance of a geotextile from a soil layer $P_{ult}$ can be predicted using the following
450 effective stress-based equation (Berg et al. 2009):

$$P_{ult} = C\ \sigma_v'\ F^*\ L_e\ \alpha \tag{3}$$

451 where C is a reinforcement effective unit parameter (typically equal to 2 for geotextiles as they
452 have upper and lower interfaces with the soil), $\sigma_v'$ is the vertical effective stress at the level of the
453 geotextile, $F^*$ is the pullout resistance factor (defined here as $F^* = \tan(\delta)$, where $\delta$ is the drained
454 interface friction angle between the backfill soil and geotextile), $L_e$ is the embedment length (the
455 actual length of embedment in a pullout test or the length of geotextile in the resisting zone behind
456 the active Rankine failure surface in a MSE wall), and $\alpha$ is a scale factor to account for the non-
457 linear stress reduction over the embedded length of highly extensible reinforcements (typically
458 assumed to be 0.6 for geosynthetic reinforcements). This equation can be applied directly to infer
459 the effects of unsaturated conditions on geosynthetic pullout by incorporating the definition of
460 vertical effective stress in unsaturated soils obtained by combining Equations (1) and (2).

461 Although Equation (3) can be used to consider the impact of effective stress in unsaturated
462 soils on the pullout resistance, it does not consider the effects of thermal softening in the peak
463 shear strength observed in studies like that of Uchaipichat and Khalili (2009). As an example, the
464 trends in the peak shear strength of Bourke silt interpreted from the stress-strain curves of
465 Uchaipichat and Khalili (2009) are plotted a function of temperature for three suction values in

Figure 14. This figure shows that the peak shear strength, represented as the peak deviator stress, increases with increasing initial matric suction, and decreases approximately linearly with temperature. A thermal softening parameter μ was defined as the decrease in peak shear strength with temperature from the results in Figure 14 (units of kPa/°C), and was incorporated into Equation (3) to account for the effects of thermal softening of the soil on the pullout resistance of geosynthetics in unsaturated soils, as follows:

$$P_{ult} = C\ \sigma'_v\ F^*\ L_e\ \alpha\ (1 + \mu\ \Delta T) \quad (4)$$

where ΔT is the change in temperature at the soil-geosynthetic interface. The results in Figure 14 indicate that the value of μ decreases slightly with increasing suction, so a value of μ = -0.002 was assumed to be representative of the silt tested in this study that has an initial matric suction of approximately 60 kPa. As μ is negative, a greater value of μ will lead to a greater decrease in $P_{ult}$ with temperature.

When applying Equation (4) to predict the pullout resistance of the geotextiles in nonisothermal conditions, the effective saturation and temperature used in the definition of the vertical effective stress in Equation (2) should be the values at the soil-geosynthetic interface. Because the effective saturation was only measured at this location via sampling in the Series 2 tests, the effective stress analysis is focused on the Series 2 tests. A comparison between the predicted pullout resistance from Equation (4) and the experimental pullout resistance is shown in Figure 15. In this figure, the interface friction angle was assumed to be 80% of the internal friction angle of the silt, which led to a good match between Equation (3) and pullout resistance at room temperature. Three predicted relationships obtained from Equation (4) are shown in Figure 15: a relationship with no thermal softening (μ = 0), a relationship with the estimated value of μ = -0.002 obtained from the trends in the peak shear strength of a similar silt reported by Uchaipichat and

Khalili (2009), and a relationship with a value of $\mu$ = -0.006. The predicted relationship with a value of $\mu$ = -0.006 showed a good fit to the experimental pullout data, indicating that the amount of thermal softening was about 3 times greater than that expected from the trends in the data from Uchaipichat and Khalili (2009). This greater amount of thermal softening could be attributed to differences between the Bonny silt evaluated in this study and the Bourke silt evaluated in their study, but could also include some effects of thermal softening of the geosynthetic. It is important to note that because the effective saturation values estimated from the volumetric water content values obtained from sampling in Figure 10(c) increase with increasing temperature, the effective stress at the soil-geosynthetic interface calculated using Equations (1) and (2) decreases with increasing temperature. If the effective saturation values inferred from the dielectric sensor measurements from 13 mm below the geotextile had been used in the analysis, an increase in pullout capacity with temperature would have been predicted. This sensitivity to the location of sampling emphasizes the importance of using the soil conditions at the soil-geosynthetic interface in an effective stress analysis of the pullout resistance.

Although the results shown in Figures 13 indicate that heating of unsaturated backfill soils may have a negative impact on the pullout resistance of woven geotextiles, the trends in the pullout resistance with temperature may have been different if water vapor had not condensed at the soil-geotextile interface. The volumetric water content results from the soil layers in the Series 1 and 2 tests consistently showed drying during heating in the rest of the soil layer. This means that if the geotextile had either greater permittivity or the ability to wick water from the soil, the trends in the results may have been different. Geotextiles with the ability to wick water from unsaturated soils have been widely evaluated in the literature (Stormont and Ramos 2004; Stormont et al. 2010; Lin et al. 2018) but have not been used in reinforcement applications.

## 8. CONCLUSIONS

This study involved the investigation of the effects of temperature on the interaction mechanisms between reinforcing geotextiles and unsaturated, compacted silt. Two testing series involving different woven geotextiles in compacted silt layers having similar initial conditions indicate that the pullout resistance decreases with increasing temperature. Although heating of the soil layers led to a decrease in volumetric water content throughout most of the soil layer associated with thermally-induced water flow, it was found in the second testing series that water was accumulating at the soil-geosynthetic interface. An effective stress analysis that considered temperature effects on the soil-water retention curve and thermal softening of the peak shear strength of the backfill soil was found to match well with the experimental pullout resistance values if the unsaturated conditions at the soil-geosynthetic interface were used. Although the reductions in the pullout resistance with temperature measured in this study may not be large enough to affect the stability of MSE walls that incorporate geothermal heat exchangers, strategies to mitigate this effect should be further investigated. In particular, the role of using wicking geotextiles to remove the water that was found to accumulate at the soil-geosynthetic interface may yield improved pullout resistance with increasing temperature.

## ACKNOWLEDGEMENTS

Financial support for this research was provided by US National Science Foundation (NSF) grants CMMI-1054190 and CMMI-1230237 and is gratefully acknowledged. The views in this paper are those of the authors alone.

## NOTATION

Basic SI units are given in parentheses.

$p_{net}$ Mean net stress (kPa)

| | | |
|---|---|---|
| 534 | $p$ | Mean total stress (kPa) |
| 535 | $u_a$ | Pore air pressure (kPa) |
| 536 | $u_w$ | Pore air pressure (kPa) |
| 537 | $\psi$ | Matric suction (kPa) |
| 538 | $\chi$ | Effective stress parameter (dim.) |
| 539 | $S_e$ | Effective saturation ($m^3/m^3$) |
| 540 | $S_r$ | Degree of saturation ($m^3/m^3$) |
| 541 | $S_{r,res}$ | Residual saturation($m^3/m^3$) |
| 542 | $T_r$ | Initial reference temperature in Grant and Salehzadeh (1996) SWRC model (K) |
| 543 | $T_f$ | Final temperature in Grant and Salehzadeh (1996) SWRC model (K) |
| 544 | $\beta_0$ | Empirical constant in Grant and Salehzadeh (1996) SWRC model |
| 545 | $\alpha_{GS}$ | Fitting parameter in Grant and Salehzadeh (1996) SWRC model ($kPa^{-1}$) |
| 546 | $\lambda_{GS}$ | Fitting parameter in Grant and Salehzadeh (1996) SWRC model |
| 547 | $e_o$ | Initial void ratio |
| 548 | $S_{r0}$ | Initial degree of saturation |
| 549 | $w_o$ | Initial gravimetric water content (%) |
| 550 | $\theta_w$ | Volumetric water content ($m^3/m^3$) |
| 551 | $\Delta\theta_w$ | Change in volumetric water content ($m^3/m^3$) |
| 552 | $\theta_o$ | Initial volumetric water content ($m^3/m^3$) |
| 553 | T0 | Initial soil temperature (°C) |
| 554 | $T_{target}$ | Applied target temperature at the box boundaries (°C) |
| 555 | $T_{ult}$ | Ultimate tensile strength (kN/m) |
| 556 | $T_g$ | Polymer glass transition temperature (°C) |

| | | |
|---|---|---|
| 557 | $P_{ult,0}$ | Pullout resistance at room temperature (kN/m) |
| 558 | C | Reinforcement effective unit parameter (dim.) |
| 559 | $\sigma_v'$ | Vertical effective stress at the level of the geotextile (kPa) |
| 560 | F* | Pullout resistance factor |
| 561 | $\delta$ | Drained interface friction angle between the backfill soil and geotextile (°) |
| 562 | $L_e$ | Embedment length (m) |
| 563 | $\alpha$ | Empirical factor in pullout model (dim.) |
| 564 | $\mu$ | Thermal softening parameter (dim.) |

## 565 ABBREVIATIONS

| | | |
|---|---|---|
| 566 | SWRC | Soil water retention curve |
| 567 | SSCC | Suction stress characteristic curve |

## 568 REFERENCES

569 ASTM D6706. (2013) Standard Test Method for Measuring Geosynthetic Pullout Resistance in
570 Soil. ASTM International. West Conshohocken, PA.

571 ASTM D5334. (2014). Standard Test Method for Determination of Thermal Conductivity of Soil
572 and Soft Rock by Thermal Needle Probe Procedure. ASTM International. West
573 Conshohocken, PA.

574 Başer, T., Dong, Y., Moradi, A.M., Lu, N., Smits, K., Ge, S., Tartakovsky, D., and McCartney,
575 J.S. (2018). “Role of water vapor diffusion and nonequilibrium phase change in geothermal
576 energy storage systems in the vadose zone.” Journal of Geotechnical and Geoenvironmental
577 Engineering. 144(7), 04018038.

578 Berg, R.R., Christopher, B.R., and Samtani, N.C. (2009). Design and Construction of
579 Mechanically-Stabilized Earth Walls and Reinforced Soil Slopes – Volume I. FHWA-NHI-
580 10-024, FHWA, U.S. Department of Transportation, Washington, D.C., USA.
581 Bishop, A.W. (1959). "The principle of effective stress." Teknisk Ukeblad I Samarbeide Med
582 Teknikk, Oslo, Norway, 106(39), 859-863.
583 Bolzon, G., Schrefler, B.A., and Zienkiewicz, O.C. (1996). "Elastoplastic soil constitutive laws
584 generalized to partially saturated states." Géotechnique. 46(2), 279-289.
585 Brand, S.R., and Duffy, D.M. (1987). "Strength and pullout testing of geogrids." Geosynthetics
586 87. IFAI. Minneapolis, MI. pp. 226-236.
587 Bueno, B.S., Costanzi, M.A., and Zornberg, J.G. (2005). "Conventional and accelerated creep tests
588 on nonwoven needle punched geotextiles." Geosynthetics International. 12(6), 276-287.
589 Campanella, R.G. and Mitchell, J.K. (1968). "Influence of temperature variations on soil
590 behavior." American Society of Civil Engineers Proceedings. 94(SM3), 709-734.
591 Carpenter, D., Zhang, M., Stewart, M.A. and McCartney, J.S. (2015). "Pullout device for
592 nonisothermal response of reinforcing geosynthetics in thermally-active geotechnical
593 systems." Geosynthetics 2015. Portland, OR. Feb. 15-18. pp. 1-9.
594 Chang, D.T.T., Chang, F.C., Yang, G.S., and Yan, C.Y. (2000). "The influence factors study for
595 geogrid pullout test." Grips, Clamps, Clamping Techniques, and Strain Measurement for
596 Testing of Geosynthetics, ASTM STP 1379. 129-142.
597 Clancy, J.M., Naughton, P.J., (2011). "An experimental study of pullout resistance of a
598 multifunctional geosynthetic in fine grained fills using an innovative pullout apparatus." Geo-
599 Frontiers 2011. GSP no. 211. J. Han and D.E. Alzamora, eds. ASCE, Reston, VA, 3609–3618.

600 Coccia, C.J.R. and McCartney, J.S. (2013). “Impact of heat exchange on the thermo-hydro-
601 mechanical response of reinforced embankments.” Proceedings of GeoCongress 2013. ASCE.
602 San Diego, CA. Mar. 3-5. pp. 343-352.
603 Coccia, C.J.R. and McCartney, J.S. (2016a). “Thermal volume change of poorly draining soils I:
604 Critical assessment of volume change mechanisms.” Computers and Geotechnics.
605 80(December), 26-40. 10.1016/j.compgeo.2016.06.009.
606 Coccia, C.J.R. and McCartney, J.S. (2016b). “Thermal volume change of poorly draining soils II:
607 Constitutive modelling.” Computers and Geotechnics. 80(December), 16-25.
608 10.1016/j.compgeo.2016.06.010.
609 Esmaili, D., Hatami, K., Miller G.A. (2014). “Influence of matric suction on geotextile
610 reinforcement marginal soil interface strength.” Geotextiles and Geomembranes. 42(2), 139-
611 153.
612 Farrag, K., Acar, Y.B., and Juran, I. (1993). “Pull-out resistance of geogrid reinforcements.”
613 Geotextiles and Geomembranes. 12(2), 133-159.
614 Grant, S.A. and Salehzadeh, A. (1996). “Calculation of temperature effects on wetting coefficients
615 of porous solids and their capillary pressure functions.” Water Resource Res. 32(2), 261-270.
616 Hatami, K. and Esmaili, D. (2015). “Unsaturated soil-woven geotextile interface strength
617 properties from small-scale pullout and interface tests.” Geosynthetics Int. 22(2), 161-172.
618 Hatami, K., Granados, J.E., Esmaili, D. and Miller, G.A. (2013). “Influence of gravimetric water
619 content on geotextile reinforcement pullout resistance in MSE walls with marginal soils.”
620 Transportation Research Record. 2363, 66-74.
621 Iryo, T. and Rowe, R.K. (2005b). “Infiltration into an embankment reinforced with nonwoven
622 geotextiles.” Canadian Geotechnical Journal. 42(4), 1145–1159.

623 Jotisankasa, A. and Rurgchaisri, N. (2018). “Shear strength of interfaces between unsaturated soils
624 and compositegeotextile with polyester yarn reinforcement.” Geotextiles and Geomembranes.
625 46, 338-353.
626 Karademir, T. (2011). Elevated Temperature Effects on Interface Shear Behavior. Doctoral
627 Dissertation. Georgia Tech., Atlanta, GA.
628 Khosravi, A. and McCartney, J.S. (2012). “Impact of hydraulic hysteresis on the small-strain shear
629 modulus of unsaturated soils.” Journal of Geotechnical and Geoenvironmental Engineering.
630 138(11), 1326–1333.
631 Khoury, C.N., Miller, G.A., Hatami K. (2011). “Unsaturated soil-geotextile interface behavior.”
632 Geotextiles and Geomembranes. 29(1), 17–28.
633 Laloui, L., Olgun, C.G., Sutman, M., McCartney, J.S., Coccia, C.J.R., Abuel-Naga, H.M., and
634 Bowers, G.A. (2014). “Issues involved with thermo-active geotechnical systems:
635 Characterization of thermo-mechanical soil behavior and soil-structure interface behavior.”
636 The Journal of the Deep Foundations Institute. 8(2), 107-119.
637 Lee, H.S. and Bobet, A. (2005). “Laboratory evaluation of pullout capacity of reinforced silty
638 sands in drained and undrained conditions.” Geotechnical Testing Journal. 28(4), 370–379.
639 Lin, C., Zhang, X., and Han, J. (2018). “Comprehensive material characterizations of pavement
640 structure installed with wicking fabrics.” Journal of Materials in Civil Engineering. 04018372.
641 Lu, N., Godt, J.W., and Wu, D.T. (2010). “A closed-form equation for effective stress in
642 unsaturated soil.” Water Resources Research. 46, 1-14.
643 McGown, A., Andrawes, K.Z., and Kabir, M.H. (1982). “Load-extension testing of geotextiles
644 confined in soil.” Proceedings of the 2nd International Conference on Geosynthetics, Vol. 3,
645 IFAI, Las Vegas, Nevada, USA, August 1982, 793-798.

646 Portelinha, F.H.M. and Zornberg, J.G. (2017). “Effect of infiltration on the performance of an
647 unsaturated geotextile-reinforced soil wall.” Geotextiles and Geomembranes 45, 211-226.
648 Philip, J.R., and De Vries, D.A. (1957). “Moisture movement in porous materials under
649 temperature gradients.” Eos Trans. AGU, 38(2), 222–232.
650 Stewart, M.A. and McCartney, J.S. (2013). “An analytical model for predicting lateral face
651 deflections of thermally active mechanically stabilized earth walls.” International Symposium
652 on Design and Practice of Geosynthetic-Reinforced Soil Structures. H.I. Ling, G. Gottardi, D.
653 Cazzuffi, J. Han, F. Tatsuoka, eds. DEStech Publications. Lancaster, PA. pp. 233-242.
654 Stewart, M.A., Coccia, C.J.R., and McCartney, J.S. (2014a). “Issues in the implementation of
655 sustainable heat exchange technologies in reinforced, unsaturated soil structures.” Proceedings
656 of GeoCongress 2014 (GSP 234), M. Abu-Farsakh and L. Hoyos, eds. ASCE. pp. 4066-4075.
657 Stewart, M.A., Coccia, C.J.R., and McCartney J.S. (2014b). “Physical modeling of the thermal-
658 hydro-mechanical response of a thermally active soil-geosynthetic system.” Proceedings of the
659 10th International Conference on Geosynthetics (ICG 10). Berlin. Sep. 21-25. pp. 1-10.
660 Stormont, J.C. and Ramos, R. (2004). “Characterization of a fiberglass geotextile for unsaturated
661 in-plane water transport.” Geotechnical Testing Journal. 27(2), 1-17.
662 Stormont, J.C, Henry, K. and Pease, R.E. (2010). “Draining unsaturated soils with geosynthetics.”
663 Geosynthetics International, 17(5), 332 - 343.
664 Sun, D., Sun, W., and Xiang L. (2010). “Effect of degree of saturation on mechanical behavior of
665 unsaturated soils and its elastoplastic simulation.” Computers and Geotech. 37(5), 678–688.
666 Uchaipichat, A. and Khalili, N. (2009). “Experimental investigation of thermo-hydro-mechanical
667 behavior of an unsaturated silt.” Géotechnique. 59(4), 339-353.

668 Vega, A. and McCartney, J.S. (2015). "Cyclic heating effects on thermal volume change of silt."
669 Environmental Geotechnics. 2(5), 257-268.
670 Yoo, H., Kim, H., Jeon, H. (2007). "Evaluation of pullout and drainage properties of geosynthetic
671 reinforcements in weathered granite backfill soils." Fiber and Polymers. 8(6), 635-641.
672 Zornberg, J.G. and Kang, Y. (2005). "Pullout of geosynthetic reinforcement with in-plane drainage
673 capability." Geosynthetics Research and Development in Progress, 18th Geosynthetic
674 Research Institute Conference (GRI-18), Austin, TX, USA. 1-6.
675 Zornberg, J.G. and Mitchell, J.K. (1994). "Reinforced soil structures with poorly draining
676 backfills. Part I: Reinforcement interactions and functions." Geosynthetics International. 1(2),
677 103-148.
678 Zornberg, J.G., Christopher, B.R. and Mitchell, J.K. (1995). "Performance of a geotextile-
679 reinforced slope using decomposed granite as backfill material." Proc. of the 2nd Brazilian
680 Symposium on Geosynthetics. São Paulo, Brazil. 19-29.
681 Zornberg, J.G., Byler, B.R. and Knudsen, J. (2004). "Creep of geotextiles using time-temperature
682 superposition methods." Journal of Geotech and Geoenv. Eng. 130(11), 1158-1168.
683 Zornberg, J.G., Bouazza, A., and McCartney J.S. (2010). "Geosynthetic capillary barriers: State-
684 of-the-knowledge." Geosynthetics International. 17(5), 273–300.

685 **Table 1** Geotechnical properties of Bonny silt

| Parameter | Value |
|---|---|
| Characteristic grain diameter, $D_{10}$ | <0.0013 mm |
| Characteristic grain diameter, $D_{30}$ | 0.022 mm |
| Characteristic grain diameter, $D_{50}$ | 0.039 mm |
| Liquid limit, LL | 25 |
| Plastic limit, PL | 21 |
| Plasticity index, PI | 4 |
| Specific gravity, $G_s$ | 2.6 |
| Peak friction angle, $\phi$' | 34° |
| Grant and Salehzadeh (1996) nonisothermal SWRC parameter, $\alpha_{GS}$ | 0.16 $kPa^{-1}$ |
| Grant and Salehzadeh (1996) nonisothermal SWRC parameter, $\lambda_{GS}$ | 1.38 |
| Grant and Salehzadeh (1996) nonisothermal SWRC parameter, $\beta_0$ | -400 K |

686

687 **Table 2** Summary of reinforcing geosynthetics evaluated in the two test series

| | **Series 1: Monotonic Pullout after Heating without a Seating Pullout Load** | **Series 2: Monotonic Pullout after Heating with a Seating Pullout Load of 10% $P_{ult}$** |
|---|---|---|
| Geosynthetic designation | Geotextile A | Geotextile B |
| Geosynthetic type | Woven geotextile | Woven geotextile |
| Geosynthetic polymer | Polypropylene (PP) | Polyethylene terephthalate (PET) |
| Ultimate tensile strength, $T_{ult}$ (kN/m) | 30.6 | 70 |
| Geotextile permittivity ($s^{-1}$) | 0.05 | 0.10 |
| Polymer glass transition temperature, $T_g$ (°C) | -20 | 70 |
| Pullout resistance from compacted silt* at room temperature, $P_{ult,0}$ (kN/m) | 9.6 | 14.3 |

688 *Silt compacted to a dry unit weight of 14.2 $kN/m^3$ at a gravimetric water content of 13.9%.

689

690 **Table 3** Summary of initial soil conditions and boundary conditions in each test (average initial
691 temperatures are 23.4 °C in Series 1 and 22.5 in Series 2)

| **Parameter** | **Series 1: Monotonic Pullout after Heating without a Seating Pullout Load** | | | | **Series 2: Monotonic Pullout after Heating with a Seating Pullout Load of 10% $P_{ult}$*** | | | | |
|---|---|---|---|---|---|---|---|---|---|
| Test number | 1.1 | 1.2 | 1.3 | 1.4 | 2.1 | 2.2 | 2.3 | 2.4 | 2.5 |
| Initial void ratio, $e_o$ | 0.83 | 0.83 | 0.83 | 0.83 | 0.83 | 0.83 | 0.83 | 0.83 | 0.83 |
| Initial degree of saturation, $S_{r0}$ | 0.44 | 0.43 | 0.43 | 0.44 | 0.44 | 0.44 | 0.43 | 0.43 | 0.46 |
| Initial gravimetric water content, $w_o$ (%) | 13.9 | 13.6 | 13.4 | 13.9 | 13.9 | 14.1 | 13.8 | 13.7 | 14.7 |
| Initial volumetric water content, $\theta_o$ ($m^3/m^3$) | 20.1 | 19.7 | 19.5 | 20.1 | 20.2 | 20.5 | 20.1 | 19.9 | 21.3 |
| Initial soil temperature, $T_0$ (°C) | 22.5 | 23.8 | 23.3 | 23.8 | 23.2 | 23.2 | 22.4 | 21.8 | 21.0 |
| Applied target temperature at the box boundaries, $T_{target}$ (°C) | 20.0 | 30.0 | 40.0 | 50.0 | 23.2 | 23.2 | 30.0 | 40.0 | 50.0 |

692 *The seating pullout load was applied in all tests in this series except reference Test 2.1
693

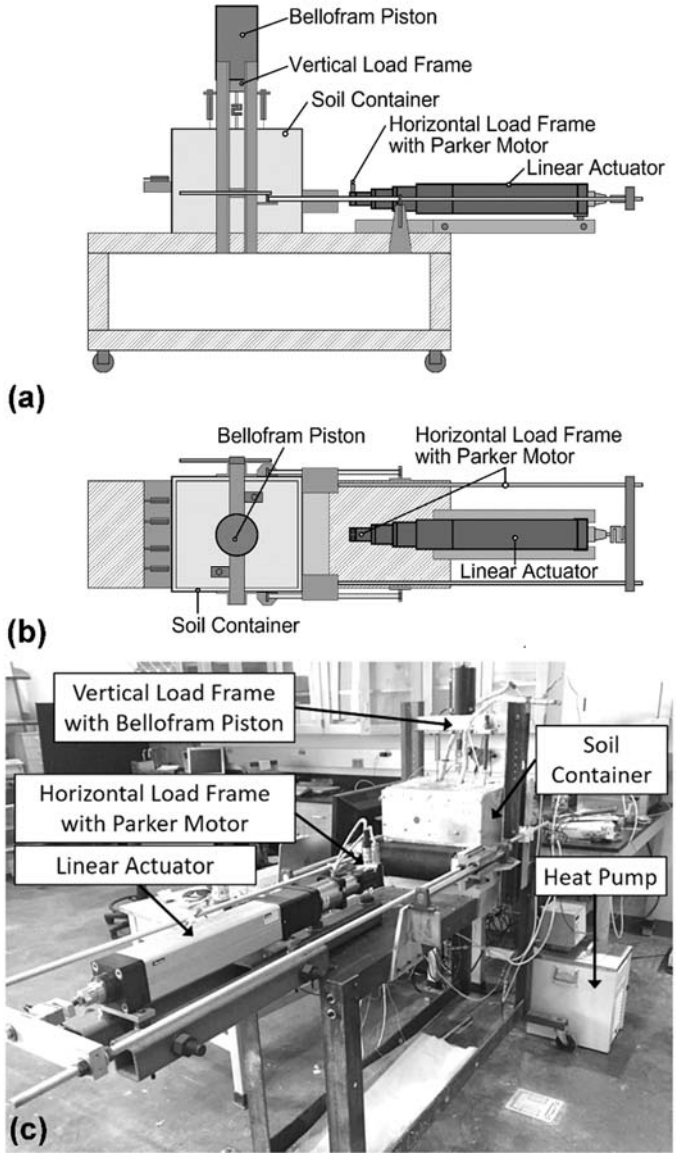


694
695 **Figure 1** Nonisothermal pullout device: (a) Elevation-view schematic; (b) Plan-view schematic;
696 (c) Picture

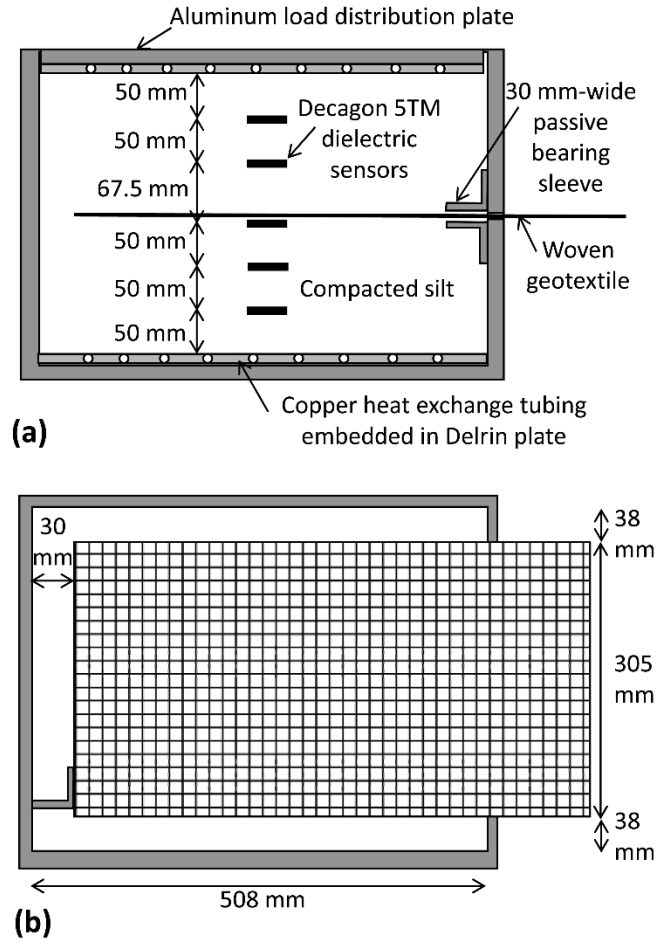


**Figure 2** Cross-sectional view schematics of the pullout device: (a) Elevation view; (b) Plan view

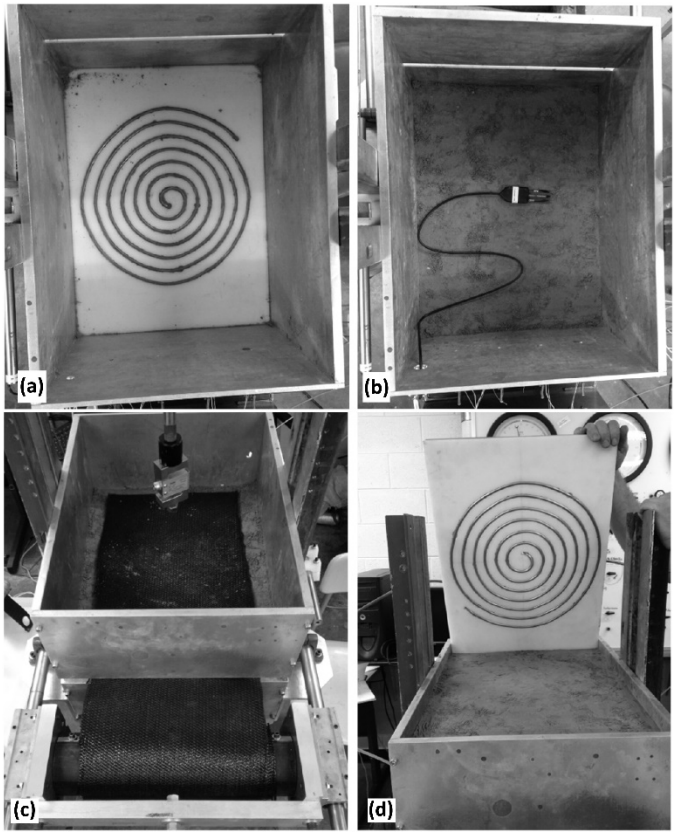


**Figure 3** Pictures of the inside of the pullout device: (a) Copper heat exchanger embedded into the lower Delrin plate; (b) Placement of typical dielectric sensor for monitoring soil temperature and volumetric water content; (c) Geotextile placement; (d) Copper heat exchanger embedded into the upper Delrin plate

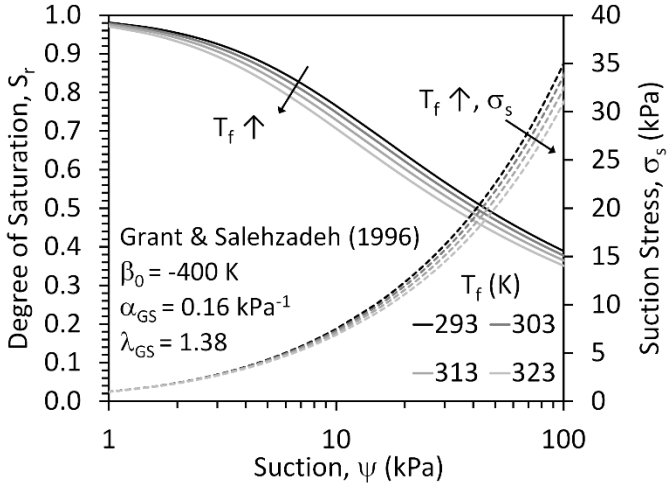


**Figure 4** Drying path soil-water retention curves (SWRCs) and suction stress characteristic curves (SSCCs) for Bonny silt under different temperatures predicted using the models of Grant and Salehzadeh (1996) and Lu et al. (2010), respectively

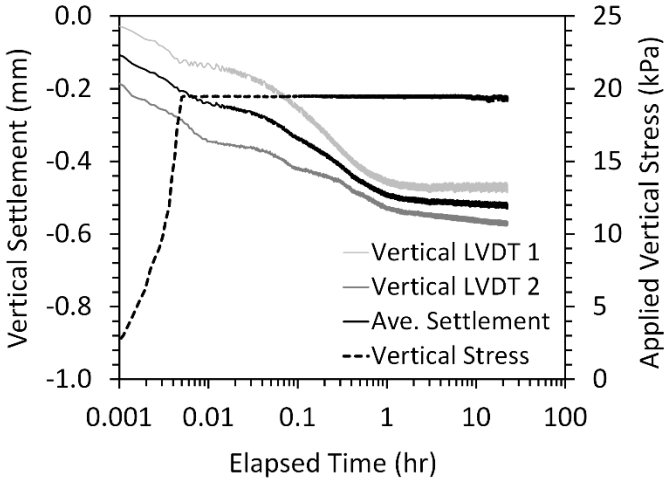


**Figure 5** Typical consolidation data for an unsaturated soil layer under the applied vertical stress

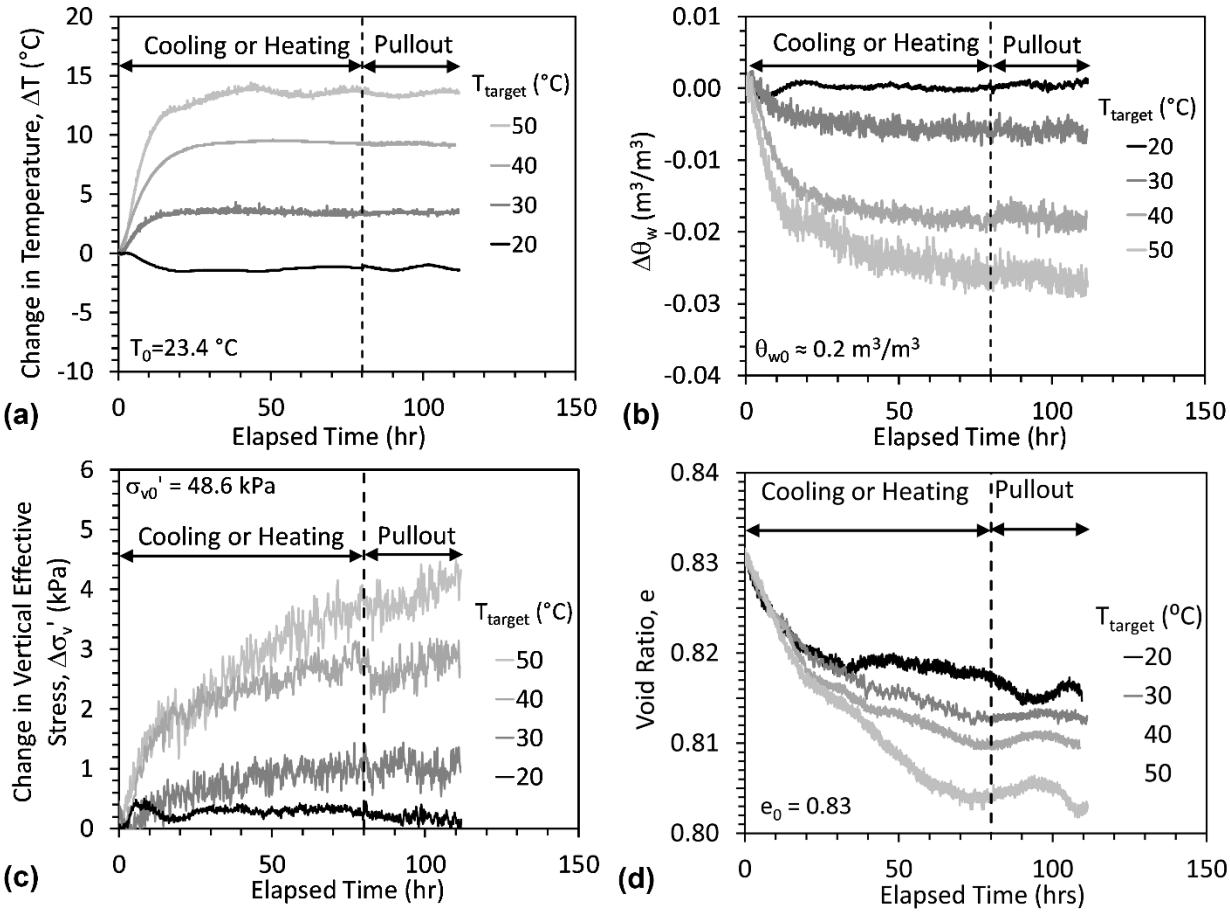


**Figure 6** Thermo-hydro-mechanical response of the soil layer in Series 1 tests for different target boundary temperatures: (a) Measured change in temperature 13 mm below the soil-geosynthetic interface versus time; (b) Measured change in volumetric water content 13 mm below the soil-geosynthetic interface versus time; (c) Calculated change in vertical effective stress 13 mm below the soil-geosynthetic interface versus time; (d) Void ratio of the soil layer versus time

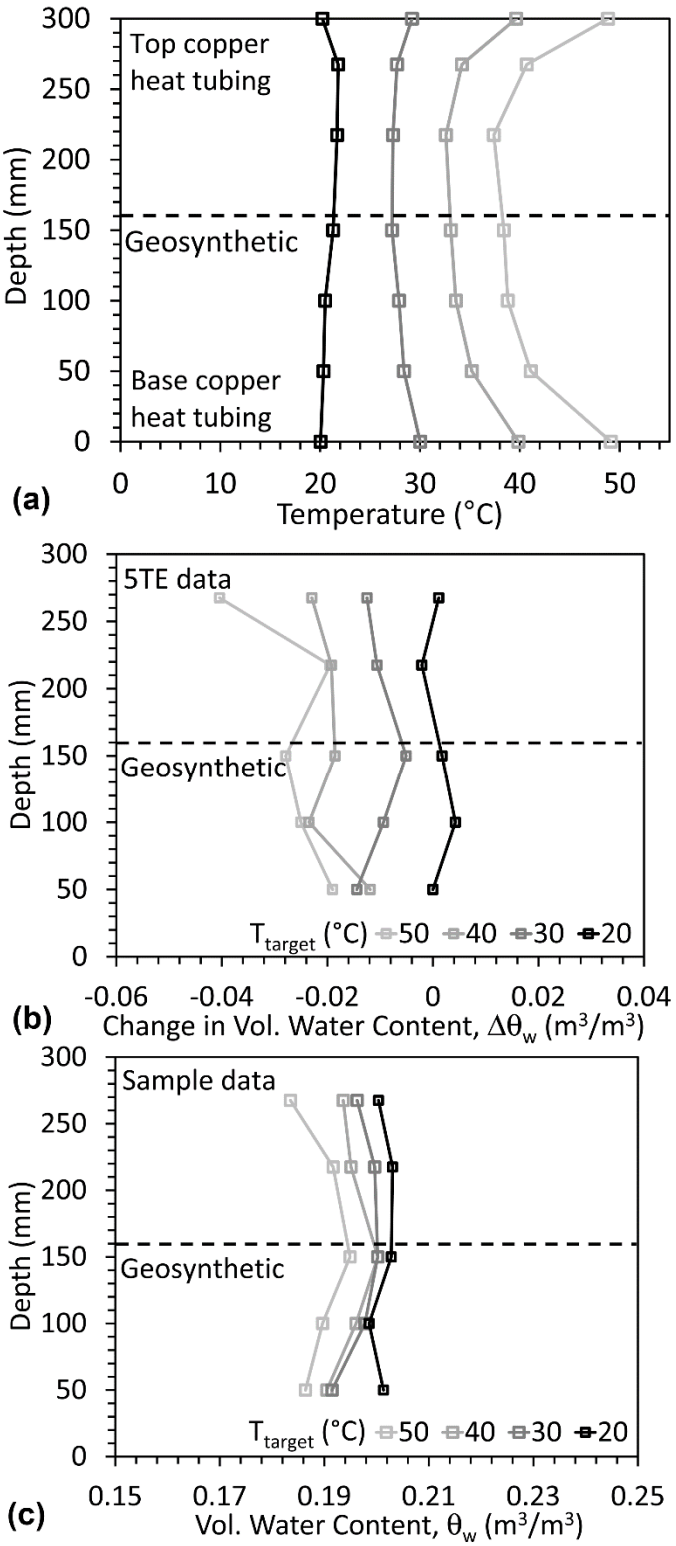


**Figure 7** Coupled heat transfer-water flow results for Series 1 tests: (a) Profiles of temperature with height in the soil layers; (b) Profiles of change in volumetric water contents from the dielectric sensors from the start of heating phase to before pullout; (c) Profiles of the average volumetric water content from oven-dried samples after pullout

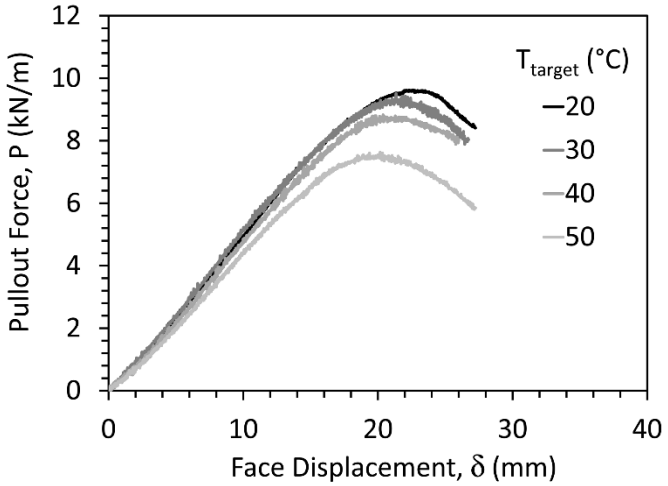


**Figure 8** Pullout force-displacement curves for Series 1 tests

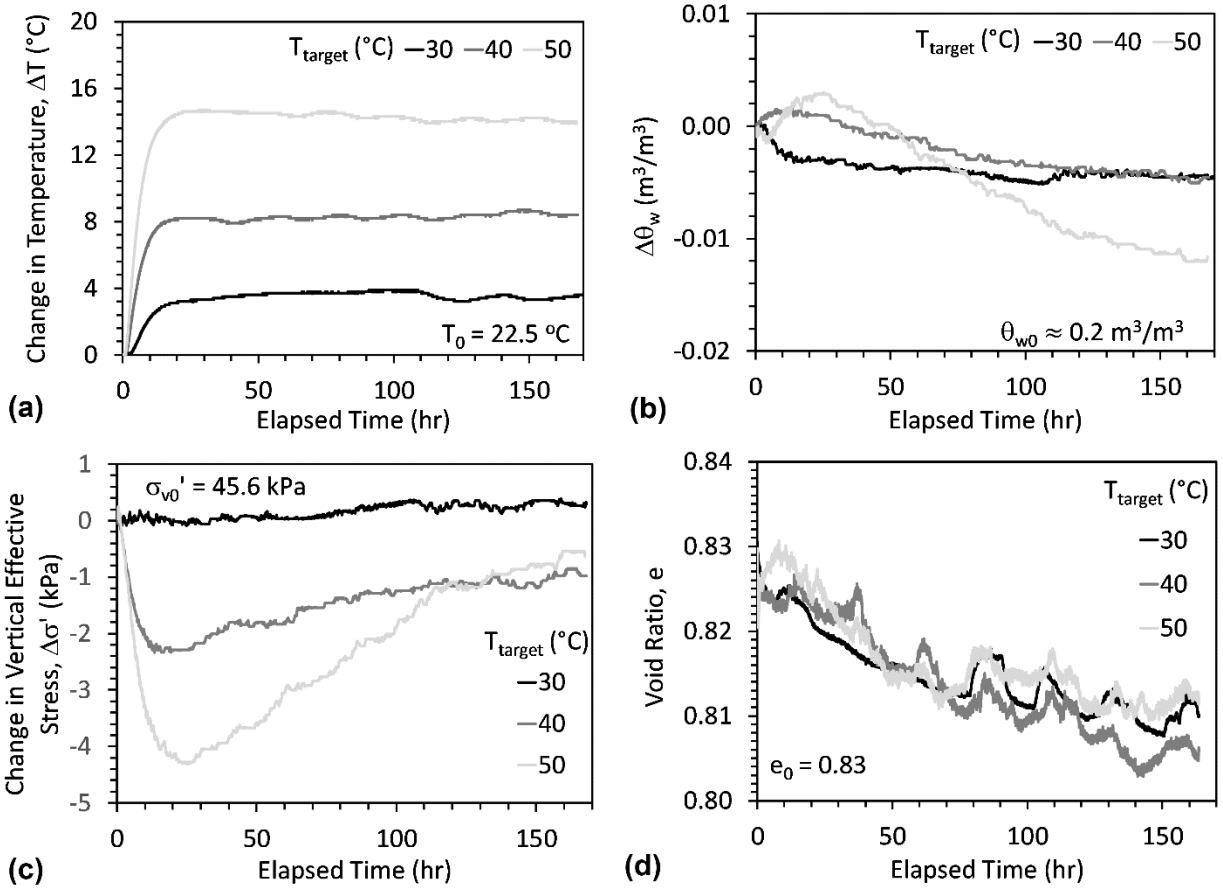


**Figure 9** Thermo-hydro-mechanical response of the soil layer in Series 2 tests for different target boundary conditions: (a) Measured change in temperature 13 mm below the soil-geosynthetic interface versus time; (b) Measured change in volumetric water content 13 mm below the soil-geosynthetic interface versus time; (c) Calculated change in vertical effective stress 13 mm below the soil-geosynthetic interface versus time; (d) Void ratio of the soil layer versus time

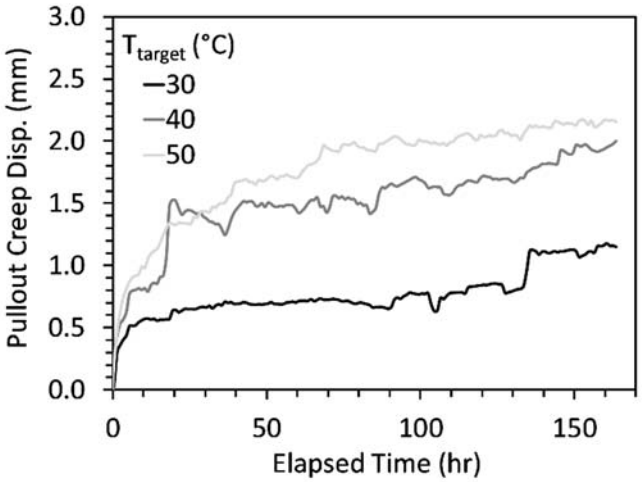


**Figure 10** Pullout creep displacements under a seating pullout load of 1.43 kN/m ($0.1P_{ult}$) for the Series 2 tests

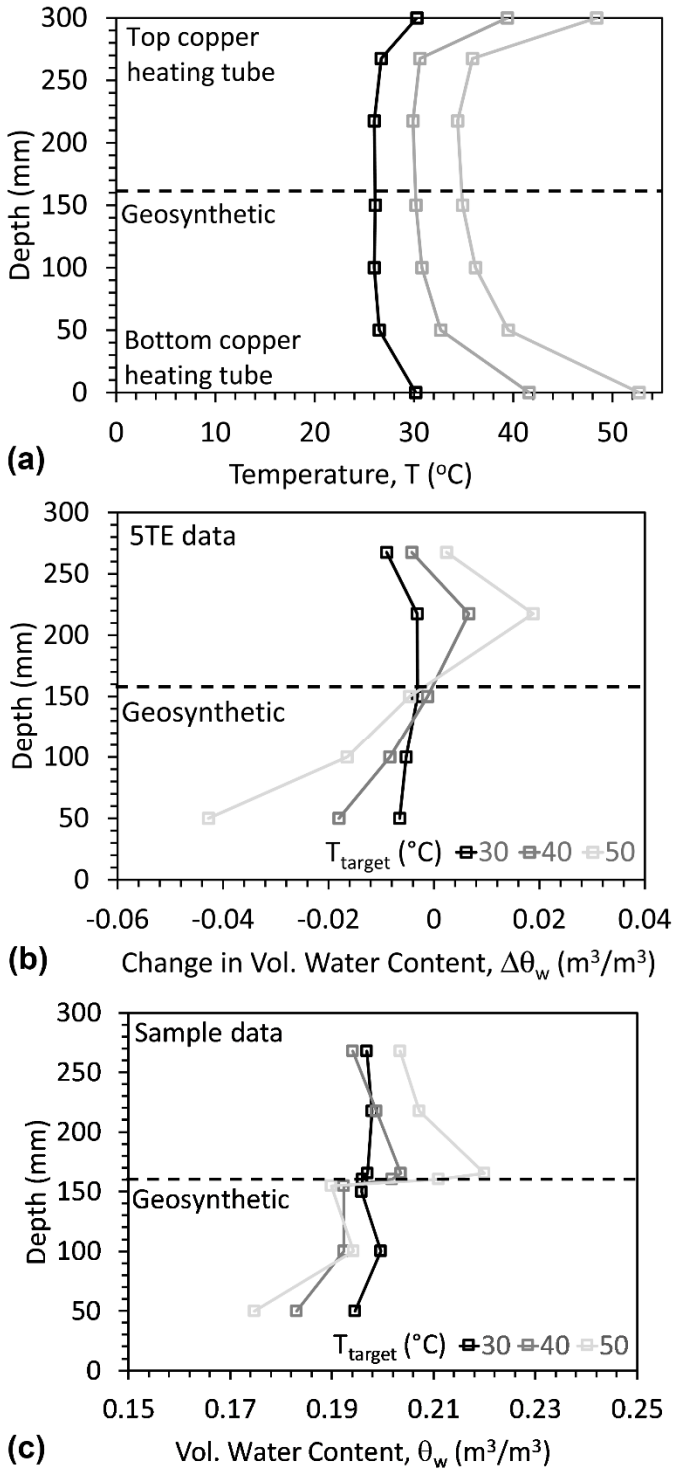


**Figure 11** Coupled heat transfer-water flow results for Series 2 tests: (a) Profiles of temperature with height in the soil layers; (b) Profiles of change in volumetric water contents from the dielectric sensors from the start of heating phase to before pullout; (c) Profiles of the average volumetric water content from oven-dried samples after pullout

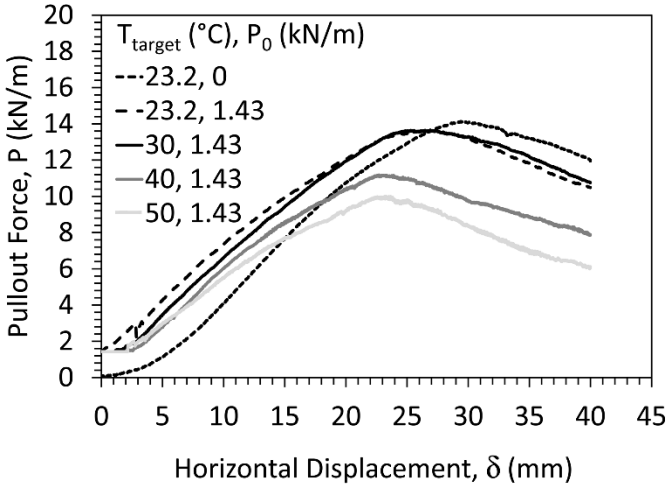


747
748 **Figure 12** Pullout force-displacement curves for Series 2 tests
749

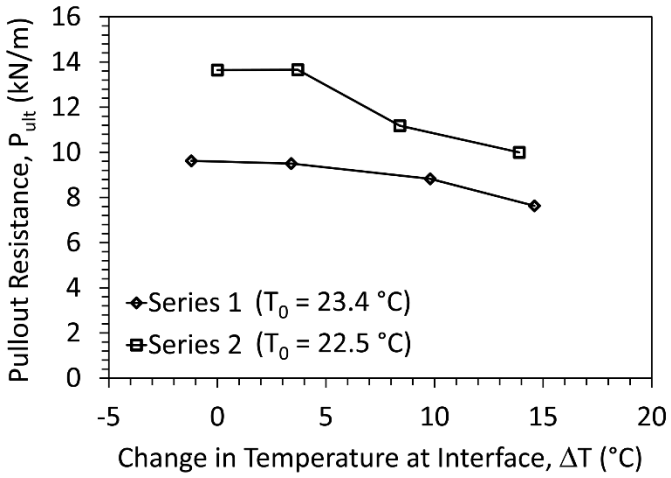


750
751 **Figure 13** Comparison of the measured pullout resistances as a function of the change in
752 temperature at the soil-geotextile interface for Series 1 and Series 2 tests
753
754
755

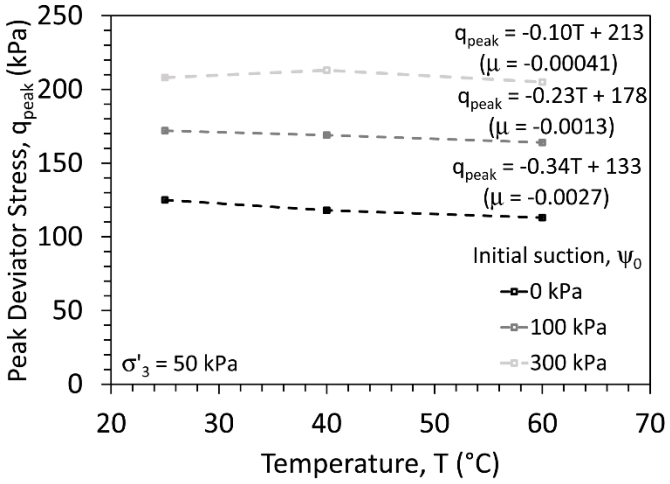


**Figure 14** Evaluation of the thermal softening of the peak deviator stress from temperature- and suction-controlled triaxial compression shear tests on Bourke Silt reported by Uchaipichat and Khalili (2009)

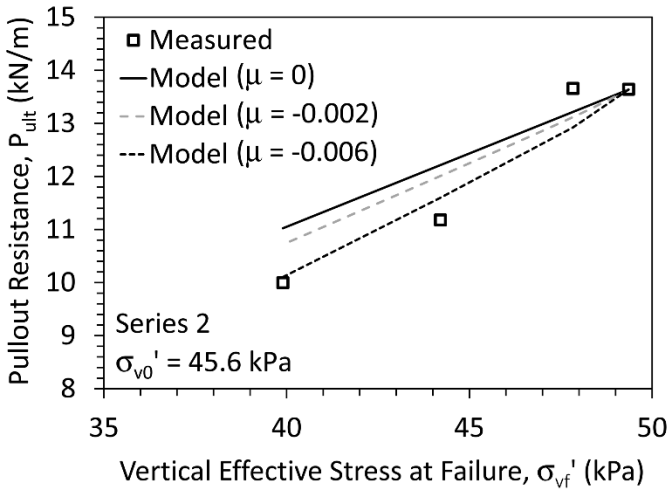


**Figure 15** Comparison of the measured and predicted pullout resistances for Series 2 tests as a function of the vertical effective stress at failure calculated using degree of saturation from oven-dried samples obtained from 0 mm above the geotextile after pullout